JOURNAL OF GEOPHYSICAL RESEARCH, VOL. 103, NO. E9, PAGES 20,149–20,158, AUGUST 30, 1998

Galileo ultraviolet spectrometer observations of Jupiter's auroral spectrum from 1600-3200 Å

Wayne R. Pryor,[1] Joseph M. Ajello,[2] W. Kent Tobiska,[3] Donald E. Shemansky,[4] Geoffrey K. James,[2] Charles W. Hord,[1] Stuart K. Stephens,[3] Robert A. West,[2] A. Ian F. Stewart,[1] William E. McClintock,[1] Karen E. Simmons,[1] Amanda R. Hendrix,[1] and Deborah A. Miller[1]

Abstract. In 1996 and 1997 the Galileo Ultraviolet Spectrometer (UVS) obtained the first measurements of Jupiter's nightside midultraviolet (MUV) polar auroral spectrum from 1620 to 3231 Å at 13 Å resolution. The reduced polar spectra, after removal of off-axis scattered radiation from the sunlit dayside of Jupiter, contain a spectrum that matches laboratory spectra of the H_2 continuum in the *a-b* dissociative emission transition. This is the first direct identification of the H_2 *a-b* transition in astronomy. The *a-b* emission is excited by electron impact exchange reactions with H_2 that peak in cross section near 15 eV. The emission threshold is at 1216 Å, and the continuum peaks in intensity in the 2000-2500 Å range. Jupiter's observed wavelength-integrated MUV H_2 *a-b* emissions (1620-3231 Å) have a photon flux ~8 times smaller than simultaneously observed wavelength-integrated far-ultraviolet (FUV) H_2 band emissions (1230-1650 Å). Because the FUV H_2 emissions have an emission cross section that peaks at higher energies near 50 eV, this FUV/MUV brightness ratio is diagnostic of the secondary electron energy distribution and is consistent with a "warm" distribution of electrons.

1. Introduction

Jupiter's aurora has been extensively studied with sounding rockets, spacecraft, and ground-based telescopes in the X ray, extreme ultraviolet (EUV), FUV, and infrared (see the review by *Ajello et al.* 1998, [this issue]). Part of the energy deposited by particle precipitation is reemitted in photons produced in transitions in H, H_2, CH_4, C_2H_2, C_2H_6, H_3^+, and other gases. Emissions in the 500-1200 Å EUV and 1200-1700 Å FUV spectral regions are due to electron and ion impact excitation of H_2 and H. Recent Galileo ultraviolet spectrometer (UVS) FUV Jupiter auroral spectra are remarkably similar to nearly simultaneous low-resolution Jupiter FUV auroral spectra obtained by J. Clarke with the Goddard high resolution spectrograph on the Hubble Space Telescope (HST) [*Ajello et al.*, this issue). Galileo EUV and FUV auroral spectra are different from an optically thin laboratory spectrum of electrons bombarding H_2 because of self-absorption effects in H_2 gas, absorption in CH_4 (methane) and C_2H_2 (acetylene), and absorption from larger hydrocarbons and from aerosols [*Ajello et al.*, this issue]. Away from the auroral regions, the poles are quite dark in the HST Wide Field Planetary Camera 2 (WFPC-2) FUV images that have some sensitivity to the MUV [*Clarke et al.*, 1996]. The hydrocarbons and aerosols that darken the FUV polar images and modify the auroral spectra are probably produced from methane by the polar auroras. The auroras contain more energy for methane dissociation than is available in sunlight for methane Lyman α photolysis in the polar regions [*Hord et al.*, 1979; *Pryor and Hord*, 1991].

The MUV auroral spectrum from 1700-3200 Å was previously unexplored because reflected sunlight from Jupiter's atmosphere overwhelms the auroral emissions as seen from the vicinity of Earth. This is not true in the EUV and FUV because the solar flux is several orders of magnitude weaker than in the MUV and because the H_2 emissions are brightest in the EUV and FUV. Galileo's unique ability to observe Jupiter's darkside has now produced the first MUV auroral spectra. This paper describes two types of MUV darkside spectra.

1. Darkside spectra of Jupiter obtained near 90° phase angle that contain off-axis scattered radiation from Jupiter's dayside, but could be obtained with a long integration period to obtain reasonable signal-to-noise.

2. Darkside spectra of Jupiter's southern aurora obtained from within the shadow of Jupiter that contain less off-axis scattered radiation from the dayside, but have low signal-to-noise.

As we will show, the 90° phase angle MUV polar auroral spectra from the nightside have a distinct wavelength-dependent emission that is not due to off-axis scattered radiation from the dayside. The MUV auroral spectrum is consistent with laboratory measurements of the H_2 *a-b* continuum radiation obtained by *James et al.* [this issue] in electron impact experiments. Simultaneous FUV/MUV spectra obtained within Jupiter's shadow clearly show bright FUV aurora but proved inconclusive in the MUV due to short integration times and a low signal-to-noise ratio.

[1] Laboratory for Atmospheric and Space Physics, University of Colorado, Boulder.
[2] Jet Propulsion Laboratory, Pasadena, California.
[3] FDC/Jet Propulsion Laboratory, Pasadena, California.
[4] Department of Aerospace Engineering, University of Southern California, Los Angeles.

Paper number 98JE00787.
0148-0227/98/98JE-00787$09.00

2. Instrumentation

The Galileo UVS instrument [*Hord et al.*, 1992] consists of a Cassegrain telescope and a Fastie-Ebert spectrometer. The spectrometer uses a scanning grating drive to obtain spectra with three different photomultiplier tubes. FUV spectra are measured with a "G" tube with a CsI photocathode in second order from 1133 to 1921 Å at 6.7 Å resolution. MUV spectra are measured from 1620 to 3231 Å with 13.6 Å resolution in first order using an "F" tube with a CsTe photocathode. Near-ultraviolet (NUV) spectra from 2820 to 4320 Å are measured with 13.6 Å resolution in first order using an "N" tube with a KCsSb photocathode. The G and N slits have the same field of view, measuring 0.1 by 1.0° on the sky. The F slit used for the MUV spectra described here is shorter in one dimension, measuring 0.1 by 0.4°. The centers of all three slits are boresighted, that is, they all look in the same direction. It requires 4 1/3 s to obtain an F-channel or G-channel spectrum, including a 1/3 s dead time for large grating motions and a 4 s interval in which smaller grating steps occur 528 times 7.57 ms apart. Actual data integration lasts 6 ms on each 7.57 ms step. Each F channel step is spectrally displaced by 3.1 Å, and samples light from a range of wavelengths 13.6 Å wide full-width at half maximum (FWHM). The F-channel recorded counts for each step are always log-compressed into 8-bit numbers by the UVS electronics. We have adopted the in-flight stellar calibration of the F-channel described by *Hendrix* [1996].

The data collection system can be configured into two modes. The recorded mode was used for observations obtained with Galileo inside Jupiter's shadow. In recorded mode each 8-bit element of data is stored separately for eventual transmission to Earth, allowing accurate reconstruction of the uncompressed tube counts at low count rates. Recorded mode is resource-intensive, requiring about 1 kbit of data to be downlinked for each second of recording.

A second mode, called real-time science (RTS), was developed in-flight when it became apparent that Galileo would be limited to low data rates by the failure of the high gain antenna deployment. RTS uses on-board summation of the instrumental data to greatly reduce the amount of downlink telemetry. For the F-channel data the general approach was to sum the log-compressed data at each wavelength in the spacecraft central computer, transmit it to the ground, and then divide by the number of integrations, decompress the data, and multiply by the number of integrations. This algorithm is satisfactory if the source observed in one integration is of constant brightness.

The UVS telescope has an external sunshade and an extensive baffle system for rejection of off-axis light. The UVS response is reduced from the on-axis response by a factor of ~10,000 for a point source 0.25° off-axis in the direction orthogonal to the long slit, and by a factor of ~30,000 at an angle of 0.5° [*Hord et al.*, 1992]. The off-axis rejection curve dictates a strategy for UVS MUV observations of observing Jupiter's aurora on the planetary darkside as far from the terminator as possible. In practice, this means observing the auroras a few slit widths (a few tenths of a degree) from the terminator on the darkside. For example, the dayside reflected light spectrum has a brightness of 9 kR/Å at the 2250 Å peak of the H_2 *a-b* continuum for the geometry in Figure 1a. (The spectrum obtained at that geometry was selected as a "reference spectrum" to represent the off-axis reflected sunlight in our reduction process.) At an angle of 0.5° the off-axis response is reduced by a factor of 30,000, so that the region of the dayside that

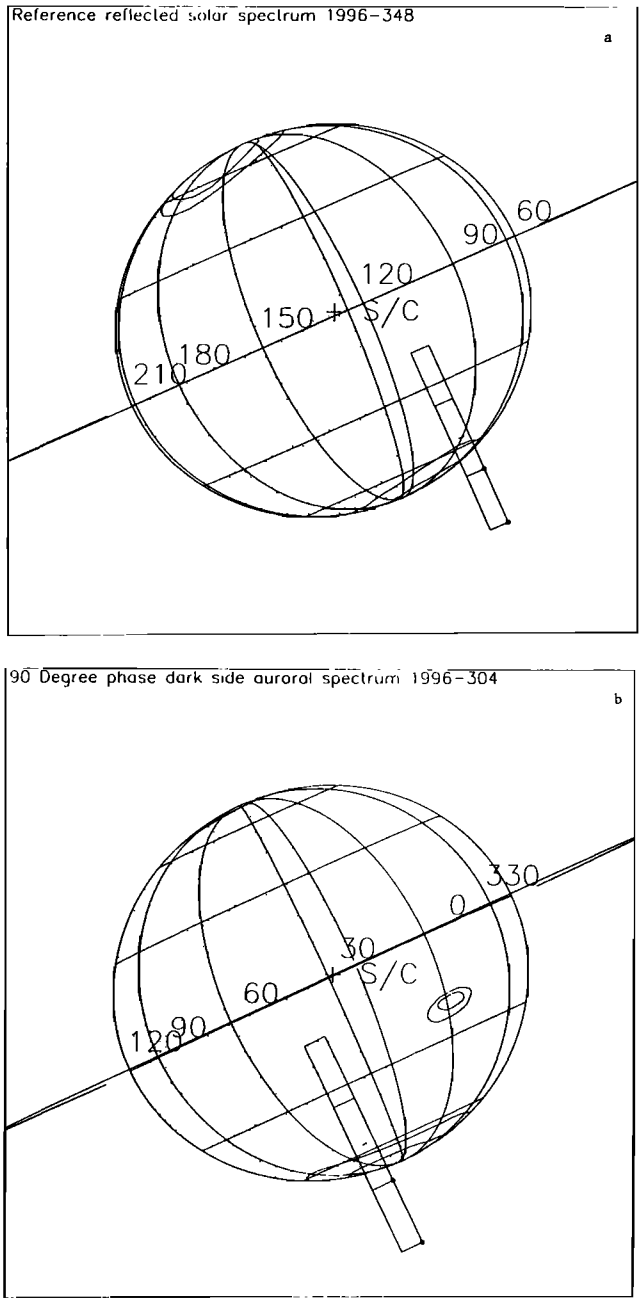

Figure 1. Galileo UVS F- and G-channel fields of view illustrated for two typical Jupiter observations near 90° phase angle. The F-channel field of view is smaller and nested inside the G-channel field of view. (a) The observing geometry for the reference reflected solar spectrum obtained on 1996 day 348 06:36-07:36 that was used in our modeling to represent off-axis scattered light. (b) A darkside auroral observation from 1996 day 304 07:38-08:07. These observations were generally done as far on the darkside as possible to minimize off-axis scattered light from Jupiter's dayside.

was on-axis for the reference spectrum contributes ~0.3 R/Å of off-axis scattered radiation to a darkside spectrum obtained 0.5° away.

3. Observations

3.1. Observations From Near 90° Phase Angle

Table 1 lists the near 90° phase angle MUV observations examined here. These were real-time observations involving

Table 1. Channel F/G Scan Observations From Near 90° Phase Angle

Day	SCE Start Time (UTC)	SCE Day	End Time (UTC)	Observation	Record	Target	System III Latitude	System III Longitude
				1996				
173	00h 07m 14s	173	00h 36m 33s	j0cd_g1aura02	2	s_term	-53.8	200.4
176	04h 14m 25s	176	04h 16m 27s	g01a_aurmap01	3	s_day	-55.3	53.0
248	00h 44m 23s	248	00h 50m 27s	g02a_aurmap01	2	s_day	-55.5	323.9
304	01h 13m 49s	304	02h 13m 28s	g02c_c3aura01	0	off planet		
	02h 14m 29s		03h 14m 08s	g02c_c3aura01	1 [a]	eq_night	-1.7	264.0
	03h 15m 09s		04h 14m 48s	g02c_c3aura01	2 [a]	eq_night	-0.2	285.2
	04h 15m 49s		05h 15m 28s	g02c_c3aura01	3	eq_night	-1.4	308.7
	05h 16m 29s		06h 16m 08s	g02c_c3aura01	4	eq_night	-2.2	334.5
	06h 17m 09s		07h 37m 01s	g02c_c3aura01	5 [b]	s_night	-55.9	19.2
	07h 38m 02s		08h 07m 21s	g02c_c3aura02	0	s_night	-57.0	45.8
	08h 08m 22s		08h 37m 41s	g02c_c3aura02	1	s_night	-54.4	55.8
	08h 38m 42s		09h 08m 01s	g02c_c3aura02	2	s_term	-54.4	64.7
	09h 09m 02s		09h 38m 21s	g02c_c3aura02	3	s_term	-55.3	76.8
308	03h 06m 21s	308	03h 17m 28s	c03a_aurmap01	2	s_day	-52.6	82.7
347	19h 25m 12s	347	20h 24m 52s	c03c_e4aura02	0 [b]	n_night	1.4	120.9
	20h 25m 52s		20h 55m 12s	c03c_e4aura02	1 [b]	n_night	65.2	203.1
	20h 56m 12s		21h 25m 32s	c03c_e4aura02	2 [b]	n_night	62.6	186.5
	21h 26m 32s		21h 55m 52s	c03c_e4aura02	3 [b]	n_night	62.5	193.5
	21h 56m 52s		22h 26m 12s	c03c_e4aura02	4 [b]	n_night	62.2	199.2
	22h 27m 12s		23h 26m 52s	c03c_e4aura02	5	n_night	61.2	204.7
347	23h 27m 52s	348	00h 27m 32s	c03c_e4aura02	6	n_term	61.4	221.3
348	02h 31m 54s		03h 31m 33s	c03c_e4aura03	1	off planet		
	03h 32m 34s		04h 32m 13s	c03c_e4aura03	2 [b]	s_night	-54.8	70.2
	04h 33m 14s		05h 32m 53s	c03c_e4aura03	3 [b]	s_night	-54.8	84.4
	05h 33m 54s		06h 33m 33s	c03c_e4aura03	4	s_night	-54.8	103.0
	06h 36m 35s		07h 36m 14s	c03c_e4aura03	5 [c]	s_day	-55.4	91.1
351	11h 33m 19s	351	11h 35m 20s	e04a_aurmap01	2	s_day	-53.9	359.1
				1997				
049	11h 43m 07s	049	12h 43m 47s	e06a_e6aura02	2	n_night	57.6	350.5
	12h 45m 48s		13h 45m 27s	e06a_e6aura03	0	n_night	61.7	37.5
	13h 46m 28s		14h 46m 07s	e06a_e6aura03	1	n_term	60.4	25.8
050	00h 57m 51s	050	01h 18m 04s	e06a_aurmap01	0	s_night	-56.6	100.8
	01h 19m 05s		01h 48m 24s	e06a_aurmap01	1	s_night	-56.5	124.6
						s_night	-55.0	94.3
092	14h 13m 10s	092	14h 42m 29s	g07a_g7aura02	1 [b]	s_night		
	15h 17m 52s		15h 47m 12s	g07a_fixtmd01	1	s_night	-55.6	74.7
	16h 49m 46s		17h 20m 13s	g07a_aurmap01	0	n_night		
	17h 21m 14s		17h 50m 33s	g07a_aurmap01	1	n_night	58.4	195.9
						n_night	56.2	181.8
	17h 51m 34s		18h 20m 53s	g07a_aurmap01	2	s_day	-67.1	149.6
	18h 21m 54s		18h 42m 07s	g07a_aurmap01	3	n_day	56.2	160.1
129	05h 05m 36s	129	06h 35m 36s	g08a_g8aura04	1	s_day	-64.4	64.4
177	07h 06m 28s	177	07h 26m 41s	c09a_aurmap03	0	s_night	-67.8	357.7
	07h 27m 42s		07h 52m 58s	c09a_aurmap03	1	s_night	-61.7	3.9
						s_term	-64.8	333.7
179	08h 38m 07s	179	09h 07m 26s	c09a_aurmap04	1	n_day	59.2	205.7
						n_day	58.6	157.9
	09h 08m 27s		09h 37m 46s	c09a_aurmap04	2	n_day	61.0	179.1

Here n_day, northern dayside, s_term, southern terminator, eq_night, equatorial darkside. All latitudes are planetocentric.

[a] Included in the darkside equatorial summed spectrum of Figure 7.

[b] Included in the darkside polar summed spectrum of Figures 5, 6, and 8.

[c] The selected reference reflected sunlight spectrum, from the south polar dayside.

alternate 4 1/3 s MUV (F-channel) and 4 1/3 s FUV (G-channel) spectral scans, called F/G scans. Some observations were darkside observations of the auroras that contain off-axis contamination from Jupiter's dayside. Some of the observations contained Jupiter's dayside and produced reflected sunlight spectra. These observations were all obtained during the period on each orbit when the spacecraft was drifting past Jupiter at about 90° phase angle. Observations from higher phase angles usually require spacecraft turns to see Jupiter and are rare because they consume spacecraft fuel. Observations at lower phase angles provided too small a view of Jupiter's dark crescent to separate the MUV aurora from the off-axis scattered light from the dayside. Lower phase angle auroral observations focused on the G channel (FUV), where the weaker sunlight does not overwhelm the aurora. The latitudes and longitudes listed are for the center of the slit. If the center of the slit fell off the body, no latitude and longitude are given. In a few cases, two pointings occurred within a single data record, both of which are given in Table 1.

A data record is one readout (flush) of the spacecraft RTS data buffer containing (in our MUV RTS data sets) a single F and a single G summed spectrum.

The geometry of the auroral ovals is not symmetric between north and south; the northern oval contains the most equatorward segment of the auroral arcs, near longitude 180°. Thus the maximum angular distance of the northern oval from the north pole viewed from Galileo is larger than the maximum angular distance of the southern oval from the south pole. This implies that the most favorable MUV observations may come from the north, when 180° is near the dark limb, providing the largest angle between the terminator and the auroral emissions in order to minimize off-axis light. Figure 1b illustrates the observing geometry for a typical darkside observation near 90° phase angle.

3.2. Observations From Within Jupiter's Shadow

On 1996 day 314 during the "Callisto 3" (C3) orbit, the Galileo spacecraft was turned to observe Jupiter's darkside from within Jupiter's shadow. UVS-recorded observations were obtained for 66 m 44 s during this turn, although only half of this was returned due to downlink limitations. The UVS observing strategy selected for the south polar observations involved alternating 4 1/3 s spectral scans of the F (MUV) and G (FUV) tubes, of which 12 m 8 s were returned. Figure 2 shows the observing geometry for the south polar observations. The F-channel slit observed darkside emissions from 100-130° System III longitude. The FUV and MUV total counts per spectrum as a function of time are shown in Figure 3. The FUV count rates peak when the slit was near the central meridian on the darkside, due to auroral emissions. The MUV count rates peak at the beginning of the observation, when the slit was pointed at the planetary limb. Figure 4 shows the summed FUV and MUV spectra for this period. The FUV spectrum shows the usual H_2 band emission pattern seen in UVS lab spectra of electron impact on H_2 [*Hord et al.*, 1992] and UVS Jupiter spectra [*Ajello et al.*, this issue]. The MUV spectrum agrees well with a least squares fit spectrum formed from a solar spectrum [*Van Hoosier et al.*, 1988] multiplied by the instrument calibration. We conclude that the MUV spectrum seen here is due to forward-scattered sunlight. A similar fit is obtained if a dayside Jupiter spectrum from UVS is used instead of a solar spectrum. Because the G slit is longer than the F slit, it is possible that the observed FUV emissions originated outside the field of view of the F slit. This low signal-to-noise data set is consistent with the absence of an MUV aurora and shows that any MUV aurora is considerably weaker than the FUV aurora.

Better MUV auroral observations were obtained at 90° phase that allow us to quantify the FUV/MUV brightness ratio. North polar observations during the C3 turn obtained by alternating the N (NUV) and G channels did not detect auroral emissions in either channel, confirming that the northern auroral oval was not in the field of view due to a late trajectory update. Additional NUV darkside observations from within Jupiter's shadow were obtained on orbit C10.

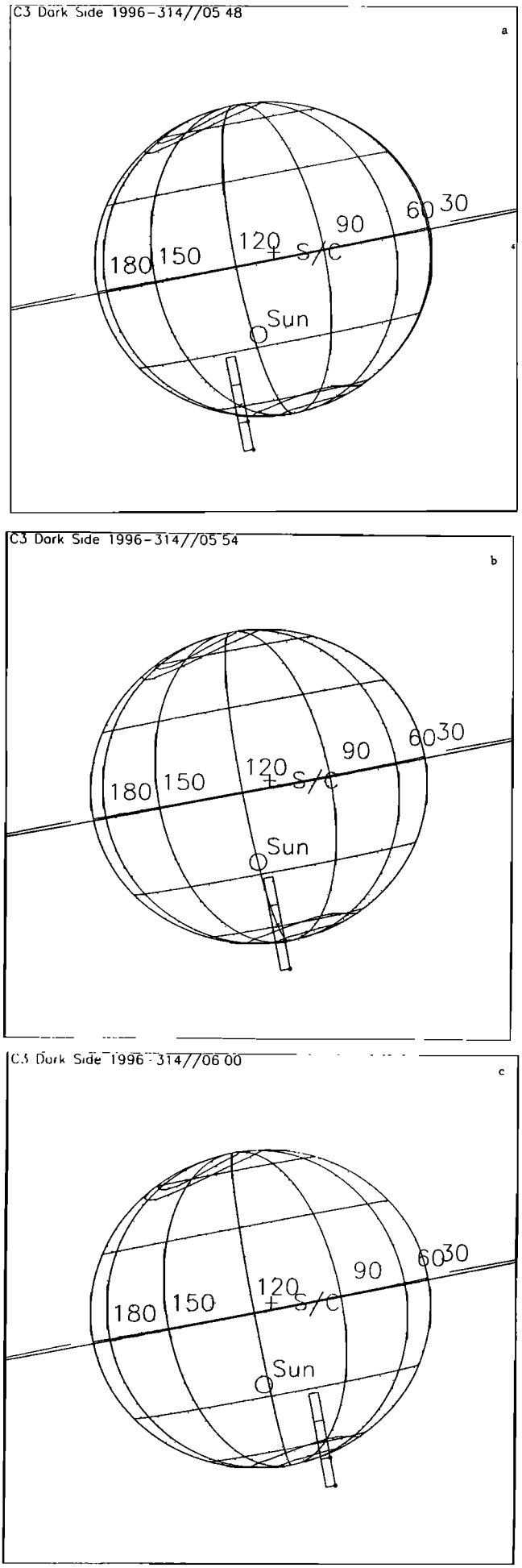

Figure 2. Viewing geometry for the F- and G-channel fields-of-view during the C3 turn south polar observations of Jupiter on 1996 day 314 05:48-06:01. Galileo was in Jupiter's shadow. The Io torus auroral oval and the more polar reference auroral oval (thought to be the source of the emissions) are shown (J. Clarke, personal communication, 1996). The geometry is shown at (a) the start (05:48), (b) the midpoint (05:54), and (c) near the end (06:00) of the observation.

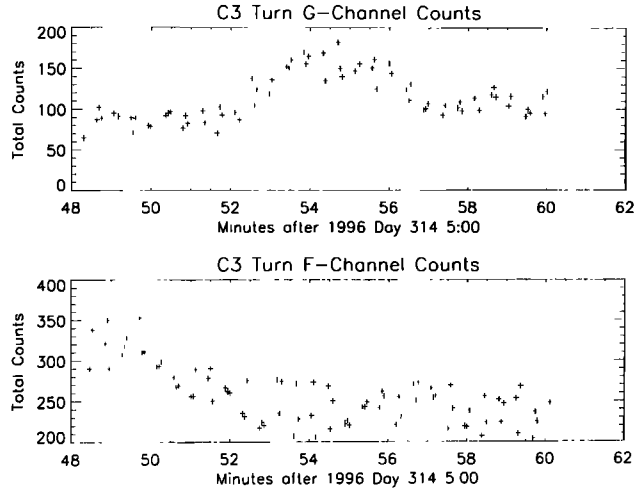

Figure 3. Total counts in each 4 1/3 s spectrum obtained in the C3 turn south polar observations indicated for (top) the FUV G channel and (bottom) the MUV F channel. Instrument background has not been subtracted.

3.3. Laboratory Spectra

Since Jupiter's atmosphere is mostly H_2 gas, we compare the Jupiter MUV auroral spectrum to the MUV spectrum emitted by electrons bombarding H_2 gas. *Ajello et al.* [1988, 1989] constructed an electron gun with magnetic collimation. The electron beam is crossed with a low-pressure gas beam, exciting various molecular and atomic emissions. *James et al.* [this issue] used this instrument with H_2 as the target gas and obtained calibrated emission spectra in the wavelength range 1750-5300 Å using electron energies of 14, 19, and 100 eV. *James et al.* identified the emissions from 1600 to 3200 Å as the H_2 *a-b* continuum band system that radiates at wavelengths longer than 1216 Å [*Ajello and Shemansky*, 1993]. The H_2 triplet $a\ ^3\Sigma_g^+$ state is excited from singlet ground state $X\ ^1\Sigma_g^+$ by the only efficient mechanism for populating the triplet structure, electron exchange collisions with low-energy free electrons. The $a\ ^3\Sigma_g^+$ state may be excited directly from the ground state, or by excitation of higher triplet states (also by electron exchange) that subsequently cascade to the $a\ ^3\Sigma_g^+$ state. The threshold energy for excitation of the $a\ ^3\Sigma_g^+$ is 11.82 eV. Below 20 eV electron impact energy, electron exchange is the most likely process for excitation of the *a* state in (1). The excited $a\ ^3\Sigma_g^+$ state radiates in an electric dipole transition to the repulsive $b\ ^3\Sigma_u^+$ state, producing H_2 *a-b* continuum emission longward of 1216 Å and two fast H(1*s*) atoms each with a few eV of kinetic energy. The combined (direct + cascade) emission cross section to the $b\ ^3\Sigma_u^+$ is rather narrow (7 eV FWHM). The emission cross section has a maximum value of 5.0 x 10^{-17} cm^2 (1.73±0.85 x 10^{-17} cm^2 due to direct excitation and 3.3x10^{-17} cm^2 due to cascade) at an electron impact energy of 15.5 eV [*Ajello and Shemansky*, 1993], in the range of values characteristic of secondary auroral electrons [*Opal et al.*, 1971]. At higher energies above 50 eV the cross section falls as $1/E^3$. Primary auroral particles have typical energies of tens or hundreds of keV. At these energies, the primaries have negligible cross section for excitation from the $X\ ^1\Sigma_g^+$ to $a\ ^3\Sigma_g^+$ state. The direct excitation and emission process can be summarized as follows [*Ajello and Shemansky*, 1993]:

$$H_2(X\ ^1\Sigma_g^+) + e \rightarrow H_2(a\ ^3\Sigma_g^+) + e \quad (1)$$

$$H_2(a\ ^3\Sigma_g^+) \rightarrow H_2(b\ ^3\Sigma_u^+) + h\nu \quad (2)$$

$$H_2(b\ ^3\Sigma_g^+) \rightarrow 2\,H(1s) \quad (3)$$

Two-photon continuum emission [*Osterbrock*, 1974] from metastable H(2*s*) atoms (lifetime against decay=0.12 s) produced by dissociative excitation of H_2 is not considered here because of rapid quenching by atomic and molecular hydrogen ions, by electrons, and by neutrals in the auroral deposition region. In this two-photon system, the probability of a 2*s* H atom becoming a 1*s* H atom by emitting a photon is symmetric around the emission peak at 2431 Å. Bound-free and free-free emission continua in H are also present in hot H, [*Osterbrock*, 1974] but are probably relatively weak emissions on Jupiter because of the low H/H_2 ratio expected at auroral altitudes and temperatures.

4. Comparison of 90° Phase Data and Model

We now describe the process of separating the nightside auroral spectrum from the somewhat brighter off-axis scattered radiation from Jupiter's dayside. Inspection of the data set suggests that darkside spectra are generally similar to the dayside reflected light spectra, but the darkest darkside polar spectra have a somewhat different spectral appearance, suggesting the presence of an auroral component. To improve the signal-to-noise ratio, we summed darkside polar observations that had relatively small radiation background and off-axis scattered radiation signatures. Figure 5 shows the sum of the north and south polar darkside MUV spectra obtained near 90° phase to date, with the selection criterion that the count rate in channel 420 at 2910 Å, near the peak of the Jupiter dayside spectrum, was below 50 counts/s. Nine records of data met this criteria

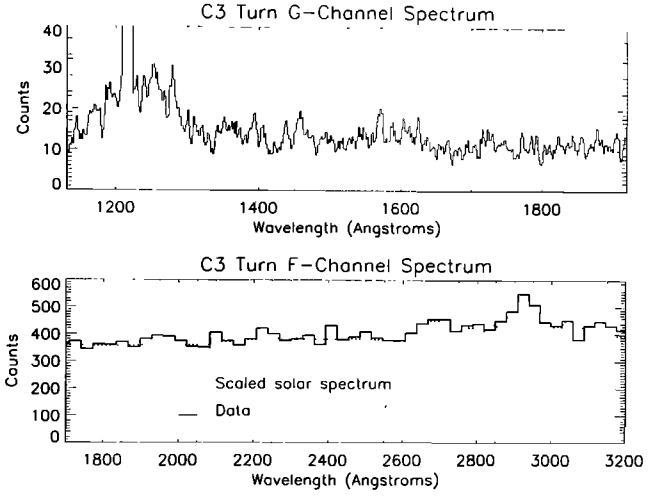

Figure 4. Summed spectra for the C3 turn south polar observations shown (top) for the FUV G channel and (bottom) for the MUV F channel. The G-channel spectrum, shown as counts per wavelength step, shows H Lyman α (1216 Å) and H_2 band emissions. The F-channel spectrum is very similar to a solar spectrum that has been multiplied by the instrument in-flight calibration [*Hendrix*, 1996]. A substantial instrumental background is also present. To obtain reasonable F-channel signal-to-noise, counts from 10 neighboring wavelength steps have been co-added.

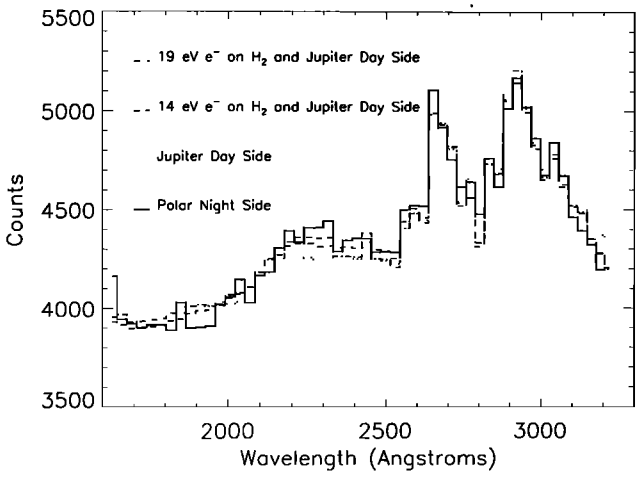

Figure 5. Summed F-channel (MUV) darkside north and south polar spectrum from 90° phase. Three multiple linear regression fits are also shown: (1) a fair fit using just a background-subtracted Jupiter polar dayside spectrum to represent the off-axis light contribution; (2) a better fit using the off-axis contribution and a 14 eV e^- on H_2 laboratory spectrum; and (3) a similar fit using the off-axis contribution and a 19 eV e^- on H_2 laboratory spectrum. To obtain reasonable F-channel signal-to-noise, counts from 10 neighboring wavelength steps have been co-added.

and are so marked in Table 1. This summed spectrum has a spectral wavelength dependence with relatively more emission at wavelengths below 2800 Å than does the dayside spectrum. We examined multiple linear regression [*Bevington*, 1969] models of this spectrum involving various regression components that included a wavelength-independent background, a reference dayside spectrum, and laboratory electron impact spectra. First, we fit the summed spectrum with only a reference dayside spectrum, where the solar reflected light is dominant and has high signal-to-noise. This regression in the software package Interactive Data Language (IDL) produces a "reduced and weighted" χ^2 of 1.13, but is a fairly poor fit, with this model larger than the data at the shortest wavelengths and smaller than the data in the wavelengths near 2300 Å where H_2 emission is expected to be visible. If the fitting function is a good approximation to the parent function, then the value of the reduced χ^2 should be approximately 1. Next, we tried a regression involving both the reference dayside spectrum and a calibrated 14 eV laboratory spectrum (multiplied by the UVS response curve). This model produces a visually appealing fit throughout the spectrum with a reduced χ^2 of 1.02. A regression with both the reference dayside spectrum and a 19 eV laboratory spectrum (multiplied by the UVS response curve) produces a somewhat worse fit, with a reduced χ^2 of 1.06. The 14 eV and 19 eV laboratory spectra are sufficiently similar that the regression program by itself could not meaningfully assess their relative contributions. Figure 6 shows the summed darkside spectrum after subtraction of (1) the solar component when the 14 eV spectrum was the other component in the regression and (2) the solar component when the 19 eV spectrum was the other component. The nonsolar component of the darkside spectrum strongly resembles the 14 and 19 eV laboratory spectra, with a somewhat better match for the 14 eV spectrum.

Examination of a summed darkside equatorial MUV spectrum (Figure 7) reveals no obvious pattern other than the off-axis dayside spectrum. The same reference reflected solar spectrum fits this spectrum with a reduced χ^2 of 1.17. In this case, adding the 14 eV or 19 eV components to the regression did not change the quality of fit χ^2 significantly: the new fits also have χ^2 of 1.17. We interpret the lack of a 14 eV or 19 eV component in the equatorial spectrum as further evidence that the high-latitude deviation in the MUV spectrum from the off-axis dayside spectrum is a phenomenon caused by the polar auroras. We also experimented with using other dayside spectra as the reference solar spectrum. While there were subtle differences between dayside spectra, the choice of spectrum did not affect the conclusion that an MUV aurora is present at high latitudes.

The significance of the MUV polar auroral detection can be discussed in several ways. The presence of a large off-axis reflected solar contribution in the spectrum raises the issue of potential systematic errors. The presence of a polar H_2 *a-b* component in the data and its absence at the equator is plausible in terms of our FUV auroral experience. Another possible concern is variations in the reflected light spectrum. We addressed these issues by varying the reference solar spectrum and continued to find the H_2 *a-b* component in the data. An additional question is the behavior of the instrument off-axis. We recently studied the UVS engineering model spectral response as a function of angle by placing Hg and D_2 lamps at the focus of a collimator to produce a plane wave at the UVS instrument. Spectra obtained with the UVS aligned with this beam (on-axis) and at an off-axis angle of 0.6° were remarkably similar in relative spectral intensity. Features did not shift in wavelength. The off-axis spectrum is much dimmer than the

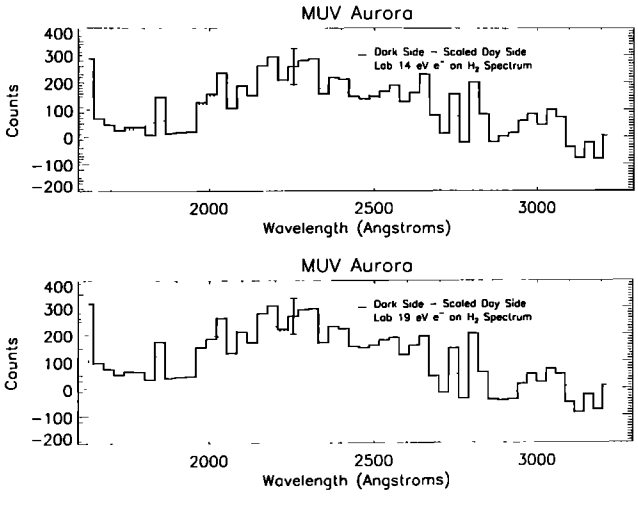

Figure 6. Jupiter darkside polar MUV spectrum from Figure 5 after subtraction of the solar contribution, leaving just the auroral component. In the upper panel, the solar part of regression (2) just described has been subtracted and is compared to the 14 eV e^- on H_2 laboratory spectrum [*James et al.*, this issue] and in the lower panel, the solar part of regression (3) just described has been subtracted and is compared to the 19 eV e^- on H_2 laboratory spectrum [*James et al.*, this issue]. The fit in the upper panel is slightly superior. Again, counts from 10 neighboring wavelength steps have been co-added. The 1-σ statistical uncertainty in the 10 grating step wide bin is shown.

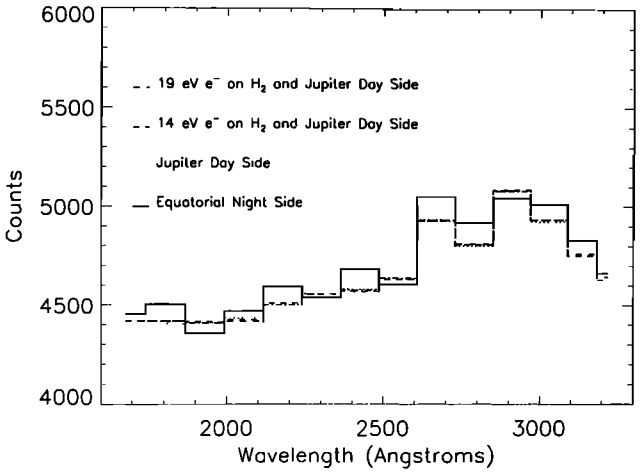

Figure 7. Summed F-channel (MUV) darkside equatorial spectrum from 90° phase. Three multiple linear regression fits are also shown: (1) a fair fit using just a Jupiter dayside spectrum to represent the off-axis light contribution, (2) an identical fit using the off-axis contribution and a 14 eV e^- on H_2 laboratory spectrum, (3) an identical fit using the off-axis contribution and a 19 eV e^- on H_2 laboratory spectrum. To obtain reasonable F-channel signal-to-noise, counts from 40 neighboring wavelength steps have been co-added.

on-axis spectrum [*Hord et al.*, 1992]. The lab work and the polar/equatorial comparison provide confidence in our data set.

The statistical significance of the detection can be discussed in two ways. First, how many standard deviations is the detection? The summed polar F-channel spectrum contains 230,772 counts, including solar reflected sunlight, instrumental background, and any signal. There are 5836 excess counts in the summed polar spectrum attributed to the H_2 *a-b* continuum. This leads to an estimated 12-σ detection. A second approach to assessing the significance of the detection involves the F-test [*Bevington*, 1969]. This technique addresses the following question: given a data set that can be fit by two components (here, the instrumental background and the reflected solar spectrum) or by three components (adding in the H_2 *a-b* continuum), how significant is the third component? Define the goodness-of-fit criterion χ^2 for a data set with N data points (N=528 here), y_i, and model points, ym_i, and statistical standard deviations σ_i

$$\chi^2 = \sum_{i=1}^{N}\left(\frac{1}{\sigma_i^2}[y_i - ym_i]^2\right)$$

and the degrees of freedom $\upsilon = N-n-1$, for a fit to a function with n coefficients plus one constant term. Then the F-test for the validity of an additional term is defined as

$$F_\chi = \frac{\chi^2(n-1)-\chi^2(n)}{\chi^2(n)/(N-n-1)}$$

For the comparison of the two-term fit to the three-term fit (with a 14 eV H_2 *a-b* spectrum) for the summed MUV polar spectrum, we find F_χ 59.9. *Bevington* [1969, Table C-5] indicates that values of $F_\chi > 10.8$ have a less than 0.001 chance of occurring by chance when the number of degrees of freedom is large. We conclude that the additional term, the 14 eV H_2 *a-b* laboratory spectrum, is significant.

5. MUV and FUV Brightnesses

The near 90° phase angle data were used to find the relative brightness of the FUV and MUV auroras. Figure 8 shows the summed FUV polar spectrum obtained simultaneously with the summed MUV polar spectrum of Figure 5. This FUV polar spectrum is similar to a 100 eV e^- on H_2 FUV spectrum obtained with the UVS in the laboratory [*Ajello et al.* 1988]. Below about 1400 Å, the spectra differ due to methane absorption from gas located above the auroral emissions and due to differences in the electron energy distribution [*Ajello et al.*, this issue]. Deliberately excluding Lyman α, we find the total number of G-channel (FUV) counts between 1230 and 1650 Å (after background subtraction) is 40,839. The total number of F-channel (MUV) counts (after subtracting a wavelength-independent background and the off-axis dayside scattered radiation contribution) is 5836. To estimate the relative emission rates requires some assumptions, because the G-channel slit is longer than the F-channel slit. If the two fields of view are filled, the wavelength-integrated signal in the G-channel (here restricted to 1230-1650 Å) is 5.8 kiloRayleighs (kR), and in the F-channel (1616.5-3227.9 Å) is 1.8 kR. In reality, the auroral arc is probably quite narrow (~200 km) in width and fills a small fraction of each slit. The actual G-channel/F-channel brightness ratio in the arc is better approximated by (5.8/1.8)(1.0°/0.4°)=8.1, where 1.0° and 0.4° are estimates for the effective slit lengths of the G and F channels, respectively. This correction is invalid if part of the emission occurs in portions of the G-channel slit that extend beyond the region of overlap with the F-channel slit. In the calibrated 14 eV e^- on H_2 laboratory spectrum the brightness ratio between G-channel (1230-1700 Å) and F-channel (1616.5-3227.9 Å) wavelengths is 1.3, at 19 eV the ratio is 2.25, and at 100 eV

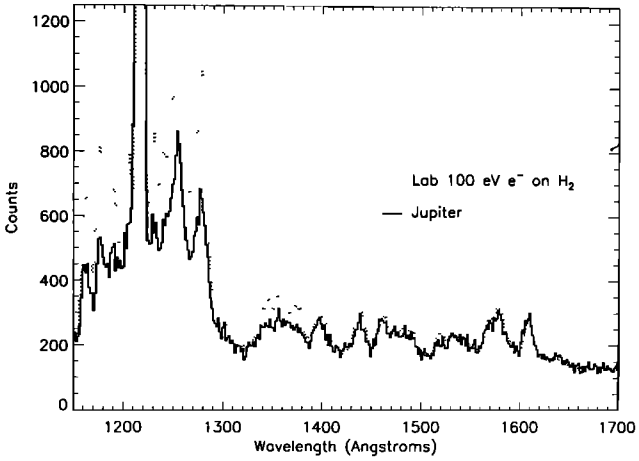

Figure 8. The Jupiter darkside FUV summed auroral spectrum obtained simultaneously with the dimmer MUV auroral spectrum in Figure 6, compared to the UVS laboratory spectrum of 100 eV e^- on H_2. Short-wavelength differences are attributed to CH_4 absorption in Jupiter's atmosphere and to electron energy effects. Note the absence of reflected solar contributions to the FUV spectrum.

the ratio is 9.9. The ratio at 100 eV is lower than that expected from the (*a-b*) model of *Ajello and Shemansky* [1993]. The unexpectedly strong H_2 (*a-b*) spectrum at 100 eV can be explained by (1) a large number of low energy secondary electrons trapped in the collimating magnetic field that efficiently excite the continuum or/and (2) a very strong cascade channel from the many upper-lying triplet states that contains a large singlet-triplet mixing. The arc-width estimate of 200 km comes from imaging of the spatially resolved arc by the Galileo solid state imager (SSI) in visible and near-infrared wavelengths (A. Ingersoll et al., Imaging Jupiter's aurora at visible wavelengths, submitted to *Journal of Geophysical Research*, 1998). The F-channel region from 1616.5 to 3227.9 Å comprises ~75% of the photons emitted in the whole H_2 (*a-b*) system (1216-∞ Å) if the spectrum is due to 14 eV electrons striking H_2.

The measured ratio of FUV/MUV brightness can be compared to theoretical expectations. The secondary electron energy distribution measured in the laboratory increases at lower energies and can be represented as a sum of 4 Maxwellians [*Opal et al.*, 1971; *Ajello et al.*, this issue]. In *Ajello et al.'s* [this issue] representation $f(E)$, the flux of secondary electrons of energy E in units electrons eV^{-1} s^{-1}, can be represented as

$$f(E) = \sum_{n=1}^{4} C_n * (E/E_n) * \exp(-E/E_n)$$

with coefficients C_n for Maxwellians of temperature T_n and energy $E_n=kT_n$ where k is Boltzmann's constant. The coefficients are C_1=2.21, C_2=0.406, C_3=2.84x10^{-2}, and C_4=9.84x10^{-4}. The corresponding temperatures in K are T_1=3.25x10^4, T_2=1.13x10^5, T_3=4.58x10^5, and T_4=2.09x10^6. This equation fits data on secondary electrons in H_2 with energies of 4-1000 eV and should not be used for lower energies. The secondary electron spectrum shape is generally independent of primary particle energy, provided one considers ejected electrons with energies considerably less than half the primary energy [*Opal et al.*, 1971]. Computing the expected brightness ratio is a matter of convolving the relevant absolute emission cross sections with the expected secondary electron spectrum. Direct electron excitation of the *B* and *C* states of H_2 responsible for the FUV *B-X* Lyman and *C-X* Werner band emission systems has a peak cross section for electrons with energies near 50 eV [*Liu et al.*, 1998]. The *a* state, responsible for the H_2 *a-b* continuum, with its narrowly peaked electron excitation cross section of 15.5 eV [*Ajello and Shemansky*, 1993], samples somewhat lower energy electrons. The convolution procedure involving model *a-b* cross sections leads to an expected FUV (1230-1650 Å)/MUV (1616.5-3227.9 Å) photon flux ratio of 2.5. The measured ratio of 8.1 is close enough to support the claimed detection. Discrepancies may reflect the different slit lengths, cross section uncertainties, secondary electron distribution differences, and the effect of hydrocarbon absorption on the FUV auroral output. We also calculate the photon flux ratio FUV Lyman (1500-1650 Å)/MUV (1616.5-3227.9 Å) because the FUV above 1500 Å has less hydrocarbon absorption [*Ajello et al.*, this issue]. In this case, we find the theoretical ratio of 1.1 and the data ratio of 3.9. The detected MUV emission is less than expected. A 27-eV Maxwellian electron distribution improves the FUV spectral shape for some auroras [*Ajello et al.*, this issue]. Convolving this proposed hotter 27-eV distribution with the cross sections gives an FUV (1230-1650 Å)/MUV (1616.5-3227.9 Å) photon flux ratio of 7.5, very close to the measured ratio of 8.1. The 27 eV photon flux ratio FUV Lyman (1500-1650 Å)/MUV (1616.5-3227.9 Å) is 3.2, very close to the data ratio of 3.9. Table 2 summarizes these ratios for the *Opal et al.* [1971] distribution, and 27 eV, 50 eV, and 100 eV Maxwellian distributions, showing the band ratios have a large sensitivity to the electron temperature. The Opal distribution is referred to as "cold", and the 100 eV monoenergetic or Maxwellian is "hot". We conclude that the FUV/MUV ratios are consistent with the presence of a "warm" auroral electron distribution, with a temperature near 27 eV. Because the slit lengths are different and the cross sections still have uncertainties near a factor of 2, this result is not yet decisive, but is suggestive of the presence of warm electrons.

6. Discussion

To the best of our knowledge, Galileo UVS has provided the first spectral observation of the H_2 *a-b* continuum emission in any astrophysical object. The H_2 *a-b* band system may be an important process for (1) heating outer planet atmospheres, molecular clouds in the interstellar medium, and stellar atmospheres of cool stars and (2) measuring the secondary electron energies. Fast atomic hydrogen H(1*s*) atoms made in the *a-b* transition with characteristic energies of 3 eV (23,000 K) will heat Jupiter's atmosphere through collisions. Diagnosing the secondary electron spectrum is also of importance because the secondaries are responsible for most of the emissions [*Rego et al.*, 1994]. It is not too surprising that the MUV auroral spectrum resembles that of H_2 excitation by electrons with 14 eV impact energy. H_2 is the most abundant gas in the Jupiter atmosphere. The manifold of triplet states of H_2 has large excitation cross sections for the *a, b, c, d, e* states in the threshold region near 15 eV [*Ajello and Shemansky*, 1993; *Khakoo and Trajmar*, 1986]. The triplet states (*c, d, e,...*) with higher excitation energy than the *a* state relax by dipole allowed radiative transitions to the *a* state, followed by an allowed transition to the *b* state. MUV spectral data are sensitive to electron energies near 15.5 eV, the peak in the *a-b* emission cross section. Simultaneously modeling the FUV and MUV brightnesses has provided an important test of the secondary electron distribution, with the surprising result that a warm electron distribu-

Table 2. Model emission ratios from different electron distributions compared to UVS data ratio.

	Photon Flux Ratio	
	FUV (1230-1650 Å)/ MUV (1616.5-3227.9Å)	FUV (1500-1650Å)/ MUV (1616.5-3227.9Å)
Galileo UVS polar data	8.1	3.9
Opal distribution	2.8	1.3
27 eV distribution	7.5	3.4
50 eV distribution	16.9	7.5
100 eV distribution	43.7	19.5

tion with energies near 27 eV is consistent with the brightness ratio.

The Galileo UVS Jupiter MUV spectra agree with the laboratory data on electron impact on H_2 quite well. However, in the FUV, substantial hydrocarbon absorptions modify the auroral spectrum substantially [*Ajello et al.*, this issue]. Reflection from below may also be important. *Yung et al.* [1982] estimated that a ~20% enhancement of the FUV Lyman bands occurs due to reflection of downward flux by Rayleigh scattering of H_2. We now consider possible corrections for MUV absorptions and reflections. The reflected sunlight spectrum of Jupiter in the MUV was measured by the International Ultraviolet Explorer (IUE) [*Wagener et al.*, 1985] and by Galileo UVS [*Hord et al.*, 1995]. At Galileo UVS resolution, the reflected sunlight spectrum is modified by the presence of aerosols, but no characteristic absorptions can be resolved. At IUE resolution, NH_3 bands are seen [*Wagener et al.*, 1985]. However, ammonia absorption occurs below the NH_3 cloud layer at the several hundred millibar level; this is well below the auroral emissions at pressures near the microbar level. Hydrocarbon and aerosol absorptions remain possible in the auroral spectrum, but based on the Galileo reflected sunlight spectrum we expect to see nearly grey continuum absorption. *Wagener et al.* [1985] modeled the IUE equatorial MUV continuum absorption from 2400 to 3200 Å with two haze layers: a 1.5 optical depth haze homogeneously distributed from 150 to 600 millibar with a constant single-scattering albedo of 0.42; and a high (50 millibar), thin (0.25 optical depth) haze of single-scattering albedo 0.97. *Wagener and Caldwell* [1988] next examined the latitude dependence of the continuum absorption in IUE spectra and found the upper haze occurs higher in the polar atmosphere, somewhere in the 0-50 millibar region. These haze layers may be below the aurora but will affect any auroral light reflected from below. IUE spectra from 2000 to 2600 Å were slightly red at high latitudes but slightly blue at the equator. These reflection spectra are sufficiently grey that correcting for the effects of absorption on the small reflected component does not significantly alter the MUV spectrum.

UVS auroral spectra of Jupiter in the still-unexplored NUV (3500-4300 Å) on orbits C3 and C10 were made with Galileo in Jupiter's shadow. We are currently studying these data, along with NUV auroral data obtained at 90° phase on orbit E6. Future measurements are planned in the Galileo Europa Mission. Initial work shows the off-axis scattered radiation problem is more severe in the NUV because of the large solar flux. NUV spectra of electrons striking H_2 gas are desirable because they have structure from allowed singlet state transitions to the *B* and *C* states, have a strong energy dependence from optically forbidden excitation to the *GK*, *H*, and *EF* states, and may be even more diagnostic of the secondary electron distribution [*James et al.*, this issue]. The Voyager camera imaged Jupiter's darkside aurora and found an intensity of ~20 kR of emission, but the emission wavelengths were not determined [*Cook et al.*, 1981]. More recently, the Galileo SSI [*Belton et al.*, 1992] has been imaging Jupiter's nightside aurora with a charged coupled device (CCD) and a variety of narrowband interference filters and finds emissions in all filters, including the NUV, the visible, and the near infrared (A. Ingersoll, private communication, 1997). A Jupiter polar orbiter mission could make good use of a spectrometer with EUV, FUV, MUV, NUV, and visible capability for simultaneously identifying the darkside emissions in optically allowed and forbidden excitation processes.

Acknowledgments. The UVS team would like to thank the Galileo flight team for making possible these unique observations. This research was supported by the NASA/JPL Galileo Project. We acknowledge helpful discussions with Randy Gladstone, Andy Ingersoll, and John Clarke.

References

Ajello, J. M., and D. E. Shemansky, Electron excitation of the $H_2(a\ ^3\Sigma_g^+ \rightarrow b\ ^3\Sigma_u^+)$ continuum in the vacuum ultraviolet, *Astrophys. J., 407*, 820-825, 1993.

Ajello, J. M., et al., Simple ultraviolet calibration source with reference spectra and its use with the Galileo orbiter ultraviolet spectrometer, *Appl. Opt., 27*, 890-914, 1988.

Ajello, J. M., G. K. James, B. O. Franklin, and D. E. Shemansky, Medium-resolution studies of extreme ultraviolet emission from N_2 by electron impact: Vibrational perturbations and cross sections of the $c_4'\ ^1\Sigma_u^+$ and $b'\ ^1\Sigma_u^+$ states, *Phys. Rev. A, 40*, 3524-3556, 1989.

Ajello, J. M., et al., Galileo orbiter ultraviolet observations of Jupiter aurora, *J. Geophys. Res.*, this issue.

Belton, M. J. S., et al., The Galileo Solid State Imaging Experiment, *Space Sci. Rev., 60*, 413-455, 1992.

Bevington, P. R., *Data Reduction and Error Analysis for the Physical Sciences*, McGraw-Hill, New York, 1969.

Clarke, J. T., et al., Far-ultraviolet imaging of Jupiter's aurora and the Io "footprint", *Science, 274*, 404-409, 1996.

Cook, A. F. II, A. V. Jones, and D. E. Shemansky, Visible aurora in Jupiter's atmosphere?, *J. Geophys. Res., 86*, 8793-8796, 1981.

Hendrix, A. R., The Galileo Ultraviolet Spectrometer: In-flight calibration and ultraviolet albedos of the moon, Gaspra, Ida, and Europa, Ph.D. thesis, Univ. of Colo., Boulder, 1996.

Hord, C. W., R. A. West, K. E. Simmons, D. L. Coffeen, M. Sato, A. L. Lane, and J. T. Bergstralh, Photometric observations of Jupiter at 2400 angstroms, *Science, 206*, 956-959, 1979.

Hord, C. W., et al., Galileo Ultraviolet Spectrometer Experiment, *Space Sci. Rev., 253*, 1992.

Hord, C. W., et al., Direct observations of Comet Shoemaker-Levy 9 fragment G impact by Galileo UVS, *Geophys. Res. Lett., 22*, 1565-1568, 1995.

James, G. K., J. M. Ajello, and W. R. Pryor, The MUV-visible spectrum of H_2 excited by electron impact, *J. Geophys. Res.*, this issue.

Khakoo, M. A., and S. Trajmar, Electron-impact excitation of the $a\ ^3\Sigma_g^+$, B $^1\Sigma_u^+$, c $^3\Pi_u$, and C $^1\Pi_u$ states of H_2, *Phys. Rev., 34*, 146-156, 1986.

Liu, X., D. E. Shemansky, S. M. Ahmed, M. Ciocca, G. K. James, and J. M. Ajello, Electron impact cross sections of the Lyman and Werner band systems of hydrogen, *Astrophys. J.*, in press, 1998.

Opal, C. B., W. K. Peterson, and E. C. Beaty, Measurements of secondary-electron spectra produced by electron impact ionization of a number of simple gases, *J. Chem. Phys., 55*, 4100-4106, 1971.

Osterbrock, D. E., *Astrophysics of Gaseous Nebulae*, W. H. Freeman, New York, 1974.

Pryor, W. R., and C. W. Hord, A study of photopolarimeter system UV absorption data on Jupiter, Saturn, Uranus, and Neptune - Implications for auroral haze formation, *Icarus, 91*, 161-172, 1991.

Rego, D., R. Prange, and J.-C. Gerard, Auroral Lyman-α and H_2 bands from the giant planets, 1, Excitation by proton precipitation in the Jovian atmosphere, *J. Geophys. Res.*, *99*, 17,075-17,094, 1994.

Van Hoosier, M. E., J. F. Bartoe, G. E. Brueckner, and D. K. Prinz, Absolute solar irradiance 120 nm-400 nm, *Astrophys. Lett.*, *27*, 163-168, 1988.

Wagener, R., and J. Caldwell, Strong north/south asymmetry in the Jovian stratosphere, *Icarus*, *74*, 141-152, 1988.

Wagener, R., J. Caldwell, T. Owen, S.-J. Kim, T. Encrenaz, and M. Combes, The Jovian stratosphere in the ultraviolet, *Icarus*, *63*, 222-236, 1985.

Yung, Y. L., G. R. Gladstone, K. M. Chang, J. M. Ajello, and S. K. Srivastava, H_2 fluorescence spectrum from 1200 to 1700 Å by electron impact: Laboratory study and application to Jovian aurora, *Astrophys. J.*, *254*, *L65*, 1982.

J.M. Ajello, G.K. James, and R.A. West, Jet Propulsion Laboratory, MS 183-601, 4800 Oak Grove Drive, Pasadena, CA 91109.

A.R. Hendrix, C.W. Hord, W.E. McClintock, D.A. Miller, W.R. Pryor, K.E. Simmons, and A.I.F. Stewart, Laboratory for Atmospheric and Space Physics, 1234 Innovation Drive, University of Colorado, Boulder, CO 80303-0590. (e-mail: wayne.pryor@lasp.colorado.edu)

D.E. Shemansky, Department of Aerospace Engineering, University of Southern California, Los Angeles, CA 90089.

S.K. Stephens and W.K. Tobiska, FDC/Jet Propulsion Laboratory, MS 264-580, 4800 Oak Grove Drive, Pasadena, CA 91109.

(Received October 1, 1998; revised March 4, 1998;
accepted March 6, 1998.)